USGS
science for a changing world

هيئة المساحة الجيولوجية السعودية
SAUDI GEOLOGICAL SURVEY

Seismic Hazard Assessment for Areas of Volcanic Activity in Western Kingdom of Saudi Arabia

Chapter P of
Active Volcanism on the Arabian Shield—Geology, Volcanology, and Geophysics of Northern Harrat Rahat and Vicinity, Kingdom of Saudi Arabia

U.S. Geological Survey Professional Paper 1862
Saudi Geological Survey Special Report SGS–SP–2021–1

U.S. Department of the Interior
U.S. Geological Survey

Cover. Photograph of Saudi Geological Survey scientists ground referencing satellite images by locating rock-wall intersections visible on satellite imagery. This and other ground-control points were used to construct a digital surface model (DSM) using satellite photogrammetry. The DSM was used for geologic mapping and hazard analysis. U.S. Geological Survey photograph by Dave Sherrod. Background image shows northern Harrat Rahat lava flows, maars, and lava domes. U.S. Geological Survey photograph by Andrew Calvert, January 25, 2012.

Seismic Hazard Assessment for Areas of Volcanic Activity in Western Kingdom of Saudi Arabia

By Hani M. Zahran, Vladimir Sokolov, and Ian C.F. Stewart

Chapter P of

Active Volcanism on the Arabian Shield—Geology, Volcanology, and Geophysics of Northern Harrat Rahat and Vicinity, Kingdom of Saudi Arabia

Edited by Thomas W. Sisson, Andrew T. Calvert, and Walter D. Mooney

U.S. Geological Survey Professional Paper 1862
Saudi Geological Survey Special Report SGS–SP–2021–1

U.S. Department of the Interior
U.S. Geological Survey

U.S. Geological Survey, Reston, Virginia: 2023

For more information on the USGS—the Federal source for science about the Earth, its natural and living resources, natural hazards, and the environment—visit https://www.usgs.gov or call 1–888–ASK–USGS.

For an overview of USGS information products, including maps, imagery, and publications, visit https://store.usgs.gov.

Suggested citation:
Zahran, H.M., Sokolov, V., and Stewart, I.C.F., 2023, Seismic hazard assessment for areas of volcanic activity in western Kingdom of Saudi Arabia, chap. P *of* Sisson, T.W., Calvert, A.T., and Mooney, W.D., eds., Active volcanism on the Arabian Shield—Geology, volcanology, and geophysics of northern Harrat Rahat and vicinity, Kingdom of Saudi Arabia: U.S. Geological Survey Professional Paper 1862 [also released as Saudi Geological Survey Special Report SGS–SP–2021–1], 18 p., https://doi.org/10.3133/pp1862P.

ISSN 1044-9612 (print)
ISSN 2330-7102 (online)

هيئة المساحة الجيولوجية السعودية
SAUDI GEOLOGICAL SURVEY

Ministry of Industry and Mineral Resources
BANDAR BIN IBRAHIM BIN ABDULLAH AL-KHORAYEF, Minister and SGS Chairman

Saudi Geological Survey
Abdullah bin Mufter Al-Shamrani, Chief Executive Officer

Saudi Geological Survey, Jiddah, Kingdom of Saudi Arabia: 2023

Contents

Figures

Tables

Abbreviations

C.E.	Common Era
cm/s^2	centimeter per second squared
DSHA	deterministic seismic hazard analysis
DTD	directional tilt derivative
GMPE	ground-motion prediction equation
km	kilometer
M	magnitude
M_L	local magnitude
M_w	moment magnitude
Ma	mega-annum
MMI	Modified Mercalli Intensity
MMN	Makkah-Madīnah-Nafud volcanic line
PGA	peak ground acceleration
PSHA	probabilistic seismic hazard assessment
SBC	Saudi Building Code

Active Volcanism on the Arabian Shield
Edited by T.W. Sisson, A.T. Calvert, and W.D. Mooney
U.S. Geological Survey Professional Paper 1862
Saudi Geological Survey Special Report SGS–SP–2021–1

Chapter P

Seismic Hazard Assessment for Areas of Volcanic Activity in Western Kingdom of Saudi Arabia

By Hani M. Zahran,[1] Vladimir Sokolov,[1] and Ian C.F. Stewart[2]

Abstract

Earthquake swarms caused by volcanic activity, tectonic stresses, or industrial operations (oil and gas production) can pose considerable risk for nearby settlements. As a rule, a probabilistic seismic hazard assessment (PSHA) that is based on time-independent earthquakes does not take into account earthquake swarms because of their statistically time-dependent nature. We describe the technique and application of a scenario-based method for the estimation of seismic hazard from earthquake swarms that may occur in areas of volcanic activity in western Saudi Arabia. The method consists of the generation of a large number of scenario seismic swarms followed by the calculation of ground motion in a site of interest for all earthquakes in all of the swarms. The set of calculated ground-motion values permits the construction and analysis of probability distribution functions for possible ground-motion levels during the hypothetical earthquake swarms. The level of ground motion representing the hazard is selected considering an appropriate value of the probability of exceedance or non-exceedance, depending on the goal of the study. This swarm-scenario-based seismic hazard assessment may provide a valuable supplement to an ordinary PSHA and (or) deterministic seismic hazard assessment that are commonly used for emergency response and post-earthquake recovery management.

Introduction

Earthquake swarms caused by tectonic stresses or by volcanic activity (Camp and others, 1987; Zobin, 2001; Moufti and others, 2013), and by industrial operation, for example, oil and gas production (Špičák, 2000), may represent a source of considerable risk for nearby settlements (Livaoğlu and others, 2017; Chen and Wolf, 2018). As a rule, the seismic risk (probability of loss from earthquakes) is estimated on the basis of a probabilistic seismic hazard assessment (PSHA) that evaluates the probability of a specific level of shaking during earthquakes. Conventionally, the seismic catalog used in a PSHA is filtered to contain time-independent events consistent with a stationary Poisson process. Thus, aftershocks and foreshocks are removed from the catalog using a procedure called "seismicity declustering" (van Stiphout and others, 2012). Because of its lack of randomness, a seismic swarm cannot be considered as a homogeneous single Poisson process. After application of the declustering procedure, the numerous seismic events in a swarm would be replaced by the single maximum magnitude earthquake.

However, declustering may lead to an underestimation of the seismic hazard (Marzocchi and Taroni, 2014), and several techniques have been suggested to incorporate earthquake clustering into a PSHA; for example, as applied to foreshock-aftershock sequences (Yeo and Cornell, 2009; Chan and others, 2013). One approach is to treat every earthquake in a particular cluster as having an independent probability of exceeding a specified level of ground motion. In this approach, the probability that ground motions from the earthquake cluster will exceed a specific level is determined through combination of these independent probabilities (Toro and Silva, 2001; Boyd, 2012). For a PSHA, it is necessary to accept the annual rate of cluster occurrence; for example, the annual rate of mainshock occurrence in a foreshock-aftershock sequence. A similar approach may be applied for earthquake swarms; however, in this case it is also necessary to estimate the annual rate of the swarms, and this step is highly uncertain because the decades-long observations needed to determine the annual swarm rate are commonly lacking.

When only the maximum magnitude earthquake in a swarm is considered, deterministic seismic hazard assessment (DSHA) is based on a specific earthquake scenario. The ground motion at the site is selected at the mean level plus one standard deviation using empirical ground-motion prediction equations (GMPEs). However, this practice, together with selection of high-magnitude scenario events and selection of the shortest source-to-site distance, suggests that DSHA may provide an unreasonably high level of estimated seismic hazard.

In this chapter, we describe the technique and application of an alternative scenario-based method for the estimation of seismic hazards from earthquake swarms. We have selected as our examples two active lava fields: Harrat Lunayyir and northern Harrat Rahat, both located in western Saudi Arabia (fig. 1). Both areas have experienced repeated volcanic

[1]Saudi Geological Survey.

[2]Stewart Geophysical Consultants Pty. Ltd.

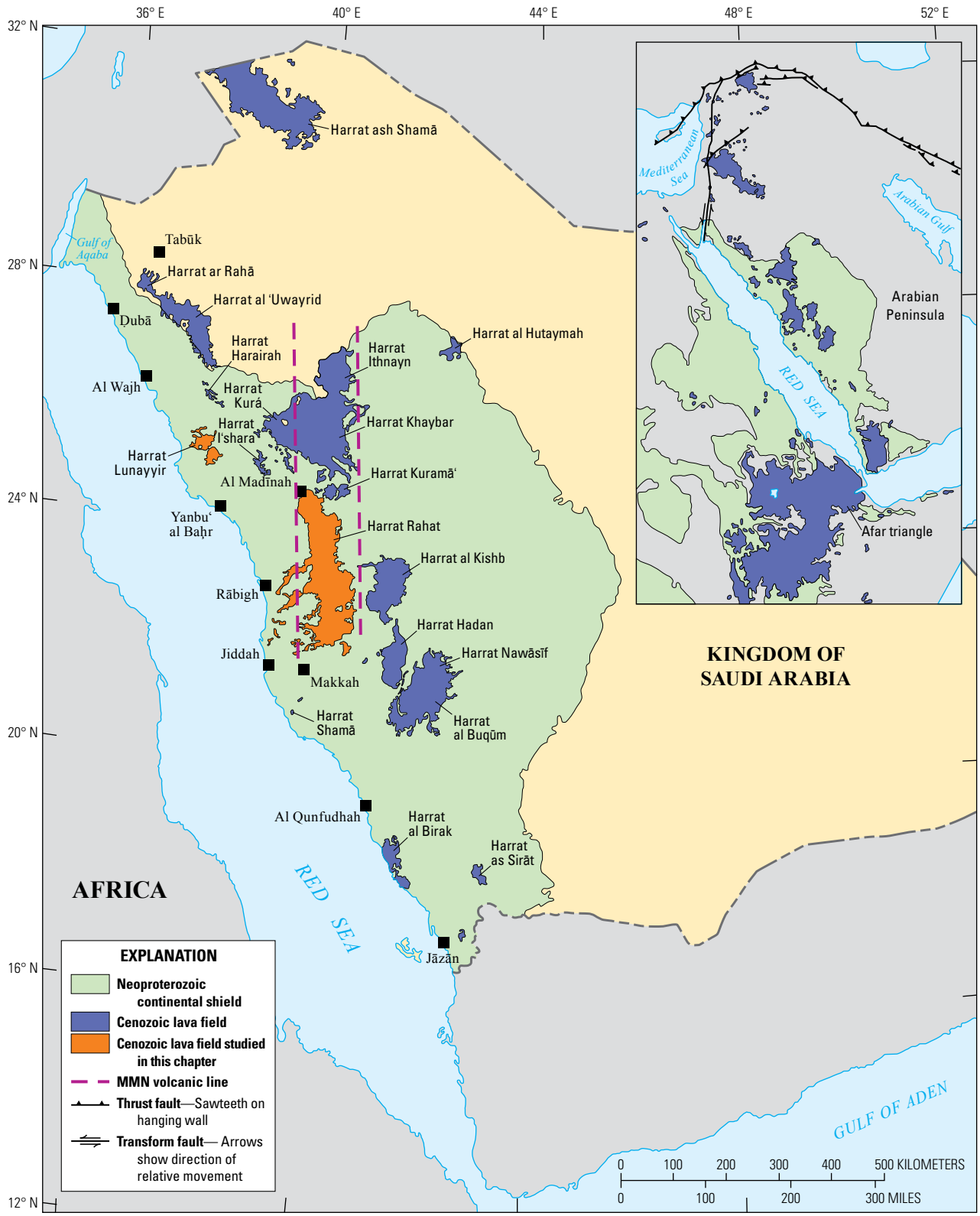

Figure 1. Map showing Cenozoic lava fields (harrats) of western Saudi Arabia (after Roobol and Al-Rehaili, 1997; not mapped outside country borders). Vertical dashed lines mark the borders of the Makkah-Madīnah-Nafud (MMN) volcanic line or lineament as defined by Roobol and Camp (1991).

activity and are characterized by episodic seismic swarm activity believed to be caused by injection of magma into the crust (Camp and Roobol, 1989; Pallister and others, 2010; Duncan and Al-Amri, 2013; Mokhtar and others, 2013). The probabilistic seismic hazard maps in the recent edition of the Saudi Building Code (SBC 301-CR-18; Saudi Building Code National Committee, 2018) consider these two areas as seismic source zones with an increased level of seismic hazard.

The technique used in this study is basically deterministic and the earthquake time dependence is not considered. The technique consists of (1) generating a large number of scenario seismic swarms with varying parameters using a Monte Carlo technique and (2) calculating the ground motion at a site of interest from all earthquakes in all swarms using selected GMPEs and corresponding random errors. The large number of accumulated ground-motion values allows for the construction and analysis of the probability distribution function and cumulative distribution function for ground-motion levels given a specific distribution of magnitudes and hypocenters of possible swarm earthquakes. The level of seismic hazard is determined using the appropriate level for the probability of exceedance (or non-exceedance) for a specific level of ground shaking (Sokolov, 2017). Note that in this case, the term "probability of exceedance" does not correspond to the term used in the PSHA, which describes the probability of exceedance during a specified period.

Input Data

The moderate level of seismicity in the western part of the Arabian Peninsula is related to spreading within the Red Sea and the active volcanism of western Saudi Arabia (Ambraseys, 1988; Moufti and others, 2013). Large areas of western Saudi Arabia are covered by lava fields (known in Arabic as harrat) (fig. 1) that formed mainly from about 10 million years ago (Ma) to recent (Camp and Roobol, 1989; Roobol and Al-Rehaili, 1997). A historical eruption was observed and recorded for northern Harrat Rahat in 1256 C.E. (Camp and others, 1987), and Harrat Lunayyir is reported to have erupted historically before 1000 C.E. (von Wissman, 1963; Brown and others, 1989; Siebert and others, 2010; Zahran and others, 2016), although supporting details are lacking. These two active zones are considered in this study, with the main focus on Harrat Lunayyir.

Harrat Lunayyir Area

In April 2009, an earthquake swarm associated with a dike intrusion began in the area of Harrat Lunayyir. The local geologic setting and characteristics of this seismic activity is analyzed in several publications (Baer and Hamiel, 2010; Pallister and others, 2010; Al-Amri and others, 2012; Duncan and Al-Amri, 2013; Mukhopadhyay and others, 2013; Abdelfattah and others, 2017, 2019; Zahran, 2017; Zahran and others, 2017; Saibi and others, 2019). Here we note that the area is characterized by relatively young (less than 600,000 years old) volcanism, with the last eruption as historical but prior to about 1000 C.E. (von Wissman, 1963; Brown and others, 1989; Siebert and others, 2010). During the period from May 15, 2009, to September 30, 2010, 19 earthquakes of magnitude (M) 4.0 or greater occurred at depths less than 20 kilometers (km), including the largest moment magnitude (M_w) 5.7 (local magnitude [M_L] 5.4) event that occurred on May 19, 2009. This earthquake caused minor damage to structures in the town of Al 'Ays located approximately 30 km from the swarm area.

Zahran and El-Hady (2017) noted that the location of the swarm corresponds to a distinct linear tectonic element—a dike that is part of the Red Sea coastal plain fault system (fig. 2; the dike corresponds to the north-northwest-oriented lineament) (Roobol and Kadi, 2008; Roobol and Stewart, 2009). This large system of nearly vertical dikes, typically 200–300 m wide, is parallel to the Red Sea coast (see fig. 7 of Zahran and others, 2016, for details). These dikes appeared during the initial phase of Red Sea rifting (Camp and Roobol, 1992). The system of dikes produces recognizable anomalies in magnetic data (Zahran and others, 2003, 2017). The location of the seismic activity indicates that a dike beneath the Harrat Lunayyir area was locally reactivated, although other sections of the dike system seem to be inactive along most of its length (at least 1,500 km).

The Harrat Lunayyir swarm occurred in a zone of intersection between the dike and local tectonic lineaments (fig. 2). Based on available geological information summarized by Al-Amri and others (2012), Zahran and El-Hady (2017) suggested that the intersection may represent the zones of weakness through which magma can ascend. Al-Amri and others (2012) interpret four young-appearing lava flows of Harrat Lunayyir to have erupted during the last 4,500 years (unit QM5 lavas; see fig. 2) but do not present evidence for that age estimate. The eruptions may have been accompanied by strong earthquakes or earthquake swarms. The recent earthquake activity in the area has shown that seismic events may also occur without lava eruption; for example, owing to dike intrusions similar to the 2009 event. The present swarm activity is concentrated in the northern part of Harrat Lunayyir, however the areas around other intersections may also be considered zones where future intrusions and corresponding earthquakes may occur.

The Harrat Lunayyir area was identified as a seismic source zone in recent studies of seismic source zonation in northwestern Saudi Arabia (Al-Arifi and others, 2013; Zahran and others, 2016; Sokolov and Zahran, 2018). Zahran (2017) inferred from seismic tomography studies that long-term volcanic and seismic activity in the area may be caused by the existence of a crustal magma conduit that transports magma from the mantle into the crust. Based on this hypothesis, Zahran and El-Hady (2017) applied a PSHA to the Harrat Lunayyir area using recent studies related to seismic source zonation (Zahran and others, 2016) and seismicity in the region (Sokolov and others, 2017). The results of the PSHA showed that the area is characterized by a significant level of hazard.

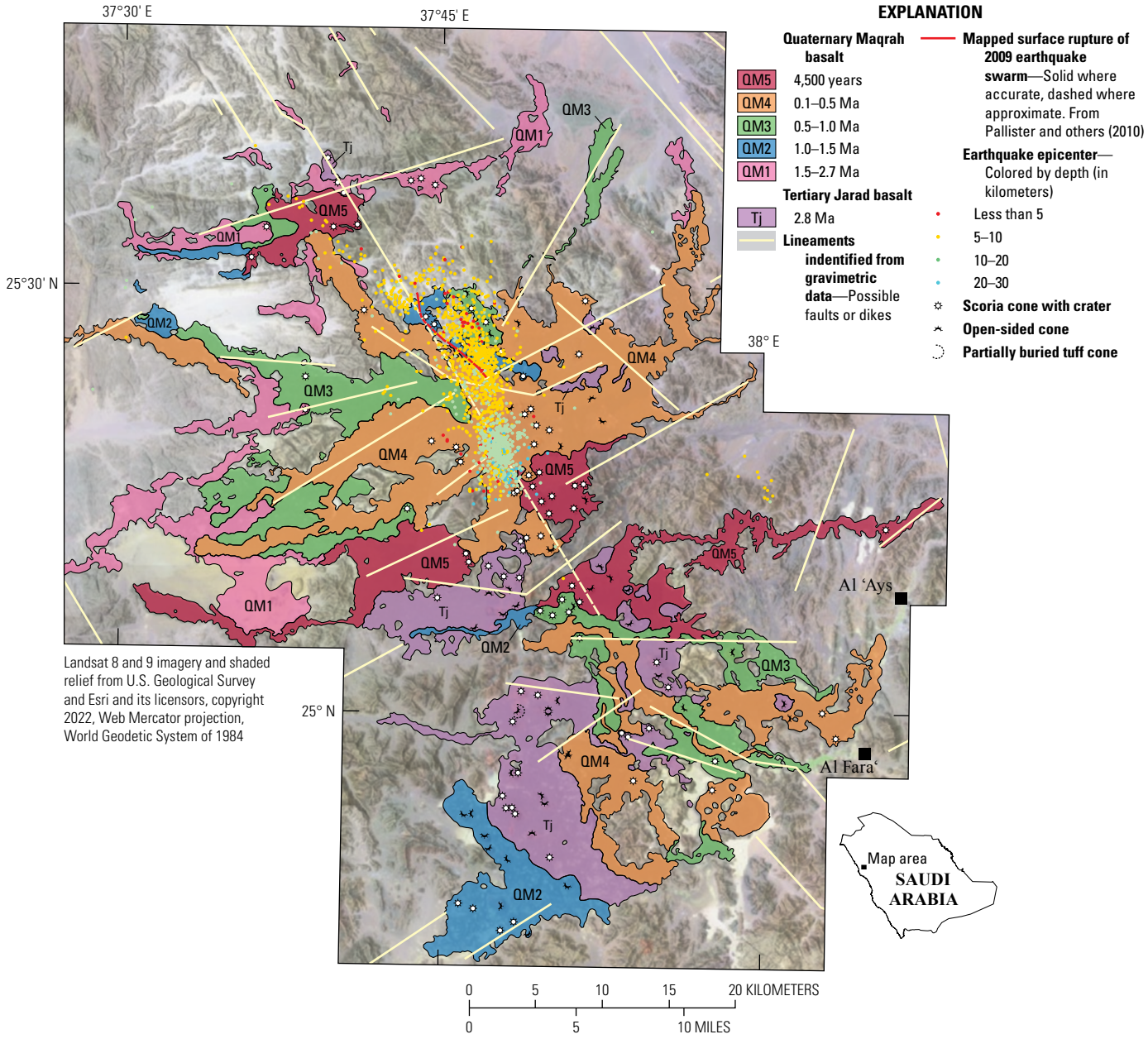

Figure 2. Map showing the geology and seismicity of Harrat Lunayyir in western Saudi Arabia during the 2009 earthquake swarm (Zahran and El-Hady, 2017). The geologic map is modified from Al-Amri and others (2012) by Zahran (2017). Lava field ages (in mega-annum [Ma]) are shown by different colors. Light yellow lines denote magnetic lineaments (possible faults or dikes; Zahran and others, 2017); the north-northwest-oriented lineament corresponds to a dike that is part of the Red Sea coastal plain fault system.

The expected peak ground acceleration (PGA) at a rock site is larger than 200 centimeters per second squared (cm/s^2) with a return period of 2,475 years for the central part of the area. The expected PGA in the town of Al ʻAys is larger than 140 cm/s^2. The probabilistic seismic hazard map in the recent edition of the Saudi Building Code (SBC 301-CR-18; Saudi Building Code National Committee, 2018) assigns PGA values of more than 140 cm/s^2 for a return period of 2,475 years (see fig. 22-3 of SBC 301-CR-18) for the Harrat Lunayyir region.

Northern Harrat Rahat

Northern Harrat Rahat (also referred to as Harrat Al Madīnah or Harrat Rashid) is an active lava field characterized by episodic seismic activity associated with the movement of magma within the crust (Abdelwahed and others, 2016; Downs and others, 2018; Stelten and others, 2020). The most recent eruption (1256 C.E.) was accompanied by swarm earthquake activity that was precursory to the eruption (Ambraseys and others, 1994). The estimated seismic intensity for the maximum earthquake in the precursory historical swarm varies from Modified Mercalli Intensity (MMI) VI (El-Masry and others, 2013) to MMI VII–VIII (Kenedi and others, 2013). A seismic swarm occurred in northern Harrat Rahat in 1999 with about 500 recorded earthquakes that had magnitudes less than 3.0 at depths of 30 to 40 km (Mokhtar and others, 2013). As noted by Stelten and others (2020), the areas with a concentration of young volcanic vents in northern Harrat Rahat are the most likely places for the next eruption and, correspondingly, for earthquake activity (fig. 3*B*). The earthquake sequence in the Harrat Lunayyir area, which is located about 225 km northwest of Al Madīnah, can be considered as an analog for possible earthquakes in northern Harrat Rahat (Kenedi and others, 2013). The probabilistic seismic hazard map in the recent edition of the Saudi Building Code (SBC 301-CR-18; Saudi Building Code National Committee, 2018) assigns PGA values of about 80 cm/s^2 (see fig. 22-3 of SBC 301-CR-18) for northern Harrat Rahat.

Langenheim and others (2019) analyzed gravity and aeromagnetic data to determine the structure of crust beneath northern Harrat Rahat. The study revealed a prominent negative gravity anomaly along and extending north of the north-northwest trending main vent axis, where the anomaly is caused in part by density variations within the underlying basement and in part by low-density volcanic rocks filling a shallow half graben. Recently Stewart and Miller (2018) showed that the directional tilt derivative (DTD) of potential field data (gravity and magnetic) is useful because of its ability to enhance linear trends with specific spatial orientations (geological faults and shear zones). As shown in figure 3*A*, several north-northwest and northeast trending lineaments were identified by Langenheim and others (2019) through analysis of the DTD of the gravity data. This analysis indicates that most of the recent and historical volcanic cones lie along the north-northwest trending faults.

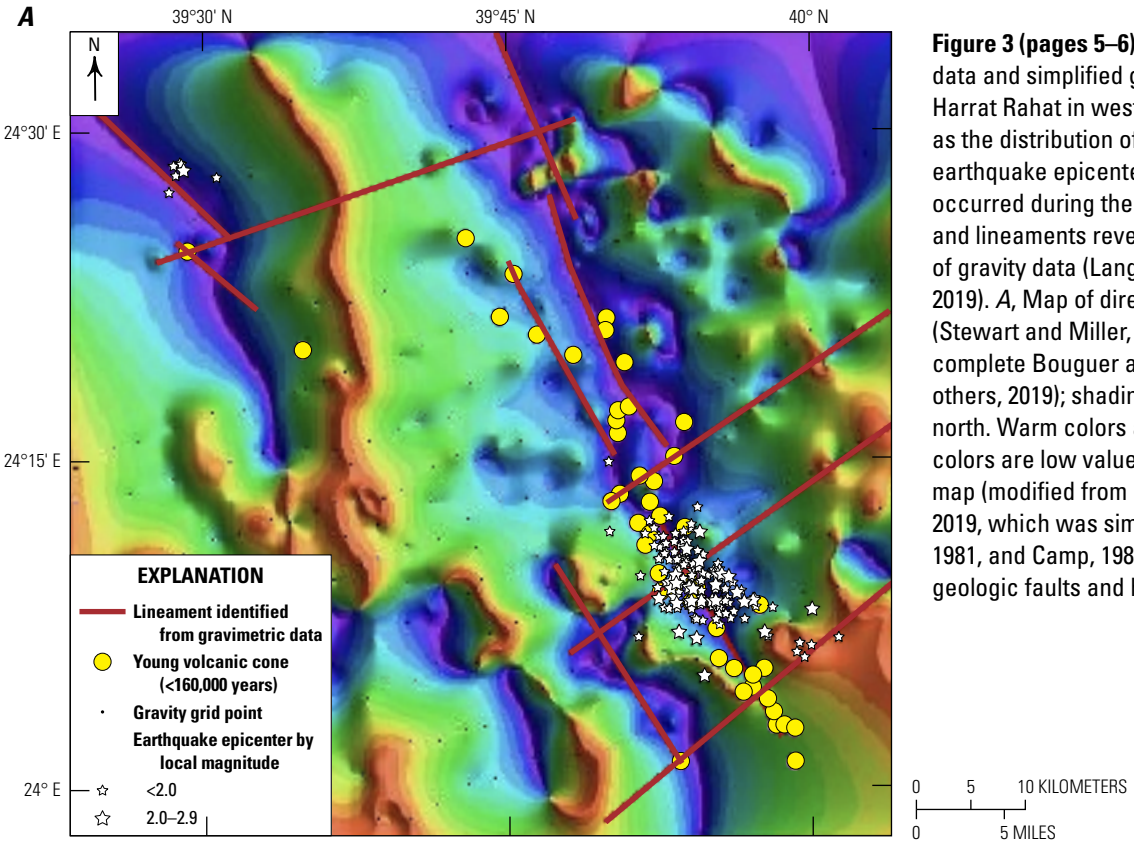

Figure 3 (pages 5–6). Maps showing gravity data and simplified geology of northern Harrat Rahat in western Saudi Arabia, as well as the distribution of volcanic cones (vents), earthquake epicenters (including those that occurred during the 1999 earthquake swarm), and lineaments revealed from analysis of gravity data (Langenheim and others, 2019). *A*, Map of directional tilt derivative (Stewart and Miller, 2018) calculated from the complete Bouguer anomaly (Langenheim and others, 2019); shading direction is 60° from north. Warm colors are high values and cool colors are low values. *B*, Simplified geologic map (modified from Langenheim and others, 2019, which was simplified from Pellaton, 1981, and Camp, 1986) showing location of geologic faults and historical vents.

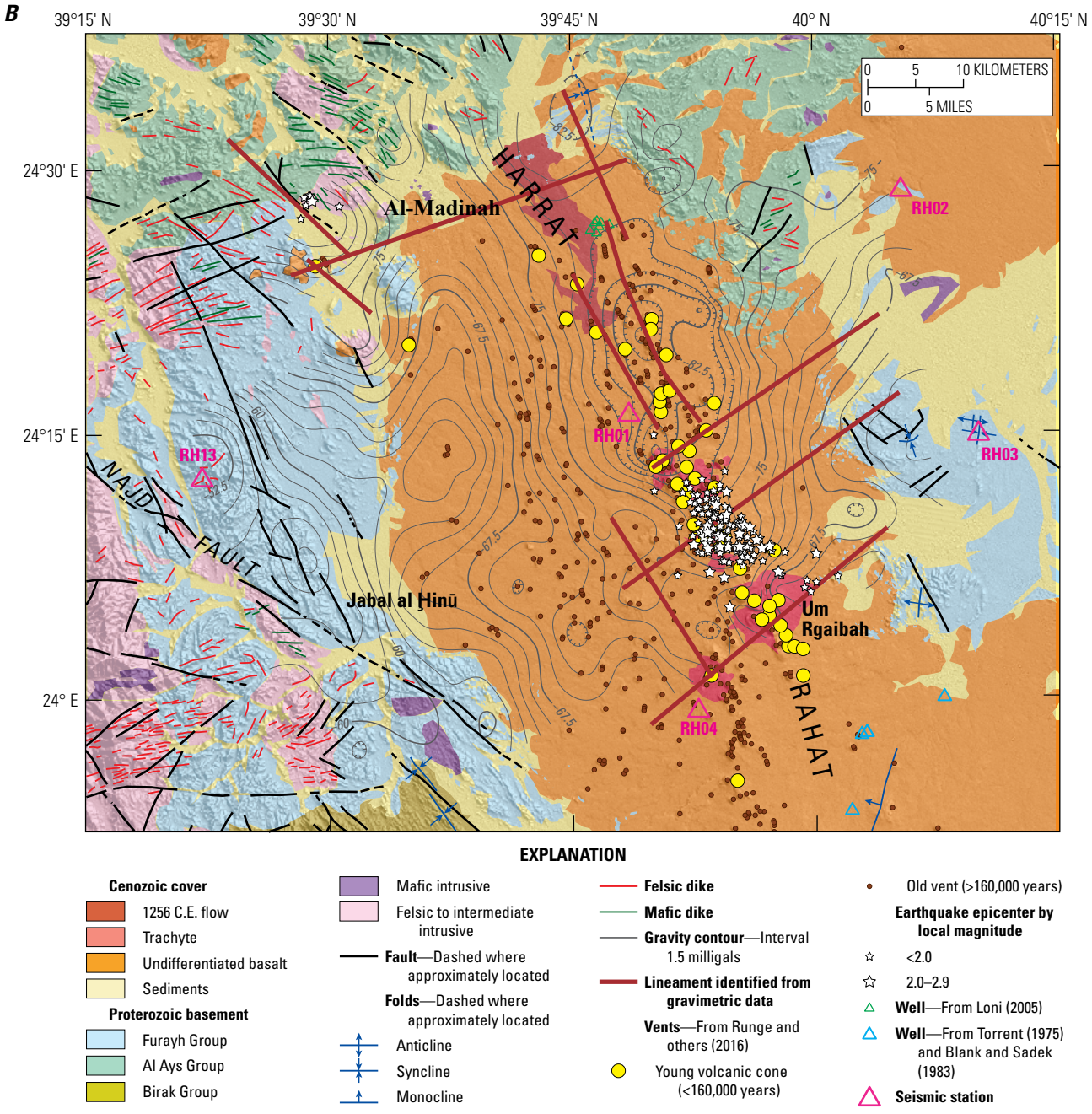

Figure 3 (pages 5–6). Maps showing gravity data and simplified geology of northern Harrat Rahat in western Saudi Arabia, as well as the distribution of volcanic cones (vents), earthquake epicenters (including those that occurred during the 1999 earthquake swarm), and lineaments revealed from analysis of gravity data (Langenheim and others, 2019). *A*, Map of directional tilt derivative (Stewart and Miller, 2018) calculated from the complete Bouguer anomaly (Langenheim and others, 2019); shading direction is 60° from north. Warm colors are high values and cool colors are low values. *B*, Simplified geologic map (modified from Langenheim and others, 2019, which was simplified from Pellaton, 1981, and Camp, 1986) showing location of geologic faults and historical vents.

Method of Seismic Hazard Analysis

The method used in this study for the estimation of seismic hazard for hypothetical earthquake swarms consists of the following steps. First, a large number of scenario swarms (referred to here as the "swarm catalog") is generated considering the characteristics of the swarm as a random variable. The primary characteristics are the (1) location of the swarm (inside the studied area), (2) volume of crust occupied by the swarm, (3) maximum magnitude earthquake in the swarm, and (4) ratio between the maximum earthquake magnitude and earthquakes with lower magnitudes. Second, the ground motion is calculated at the site of interest for each seismic event in the swarm catalog using selected GMPEs and their corresponding random errors. The ground-motion parameter (peak ground acceleration, *PGA*, in this case) for every earthquake i at every location j is estimated for every GMPE k, using the median GMPE values $ln\overline{PGA}_{i,j,k}$ and random error $\delta_{i,j,k} = \varepsilon_{i,j} \times \sigma_k$, where $\varepsilon_{i,j}$ is the randomly generated standard normal deviate (or the normalized residual) and σ_k is the standard deviation of the ground-motion parameter specified for the given GMPE.

$$PGA_{i,j,k} = \exp(ln\overline{PGA}_{i,j,k} + \delta_{i,j,k}) \quad (1)$$

Next, the weighted average is calculated as

$$PGA_{i,j} = \Sigma_{k=1}^{5}(PGA_{i,j,k} \times w_k) \quad (2)$$

where w_k is the weight assigned to each GMPE k. The set of ground-motion values calculated at given location j from all earthquakes is used to construct the probability distribution function and cumulative distribution function that represents ground-motion levels in the location during the hypothetical earthquake swarms.

Harrat Lunayyir

We use Harrat Lunayyir as an example for the description of the technique. The characteristics of the earthquake swarm that occurred at Harrat Lunayyir in 2009 (Zahran, 2017; Zahran and El-Hady, 2017) are used to generate the swarm catalog. Based on the swarm seismic activity recorded during 2007–2009 (fig. 2), it is assumed that the scenario swarms may occur inside a relatively narrow zone (a so-called dike seismic source zone) that stretches along the Red Sea coastal dike within the Harrat Lunayyir area. Following the model earthquake source zones introduced by Zahran and El-Hady (2017), three alternative models of the swarm zone are considered (fig. 4). In the first model, the earthquakes may occur along the entire section of the coastal dike located within the Harrat Lunayyir area (so-called entire fault, or the EF model). In the second model, only part of the dike with recent lava eruptions is considered (active part of the dike, the active fault, AF model). The third model assumes that earthquakes may occur only in the north segment of the dike bounded by the northeast-trending lineaments (the north fault, NF model). The weights are assigned for the alternative models following the study by Zahran and El-Hady (2017): the EF model weight = 0.3; the AF model weight = 0.5; the NF model weight = 0.2.

For the generation of the swarm scenarios, it is assumed that every scenario contains one event with maximum magnitude M_{max}, the value of which is assigned randomly within the range M_w 6.0 to 6.4 assuming a uniform distribution (Zahran and El-Hady, 2017). The lower bound value (M_w 6.0) was estimated from relations between length of the rupture along the causative fault and earthquake magnitude (Vakov, 1996). The upper bound value correlates with the maximum magnitude earthquake (M_w 5.9) observed during the 2007 Natron Rift system, Tanzania, swarm (Albaric and others, 2010), which occurred on a young (<5 Ma) segment of the east branch of the East African Rift Zone. Deformation in the Natron Rift is accommodated by normal faulting and dike emplacement (Albaric and others, 2010). Thus, the Natron Rift swarm may be considered as an analog of the Harrat Lunayyir swarm. We accept maximum magnitude on a particular seismic source as the maximum observed magnitude plus 0.5 (Kijko and Graham, 1998), such that M_w 5.9 + 0.5 = M_w 6.4. Such an approach is used in earthquake hazard assessments when neither paleoseismic evidence nor historical observations are available.

The number of smaller magnitude events, N_M, is determined using the relative ratio of small and large magnitudes that is the b-value in the magnitude-frequency distribution (Gutenberg and Richter, 1956). Based on observations of seismic activity (Mukhopadhyay and others, 2013; Abdelfattah and others, 2017), in our study the b-value is considered a random variable (normal distribution) with mean = 0.9 and standard deviation = 0.09. The minimum magnitude M_{min} of the generated earthquakes is assumed to be equal to M_w 4.0.

Table 1 shows the parameters of the model for stochastic simulation of scenario earthquake swarms. These parameters are based on the available data and studies of the 2009 Harrat Lunayyir swarm (Mukhopadhyay and others, 2013; Abdelfattah and others, 2017). The simulation is achieved using the following scheme. First, the parameters of the scenario swarm are selected randomly for every swarm generation considering the assumed distribution laws. Second, the number of earthquakes of various magnitudes (ranging from M_{min} to M_{max}) in the given swarm scenario are calculated using the random b-value assigned for the scenario. Third, the location of every earthquake inside the swarm volume with randomly generated dimensions (length, width, and depth) is assigned randomly assuming a uniform distribution along all three dimensions. The scenario swarm earthquakes are all centered within the swarm volume and have random strike directions. Note that the earthquake source parameters (length and width) that depend on magnitude are assigned randomly using the corresponding relations between magnitude and length and width (Vakov, 1996). Finally, the random location

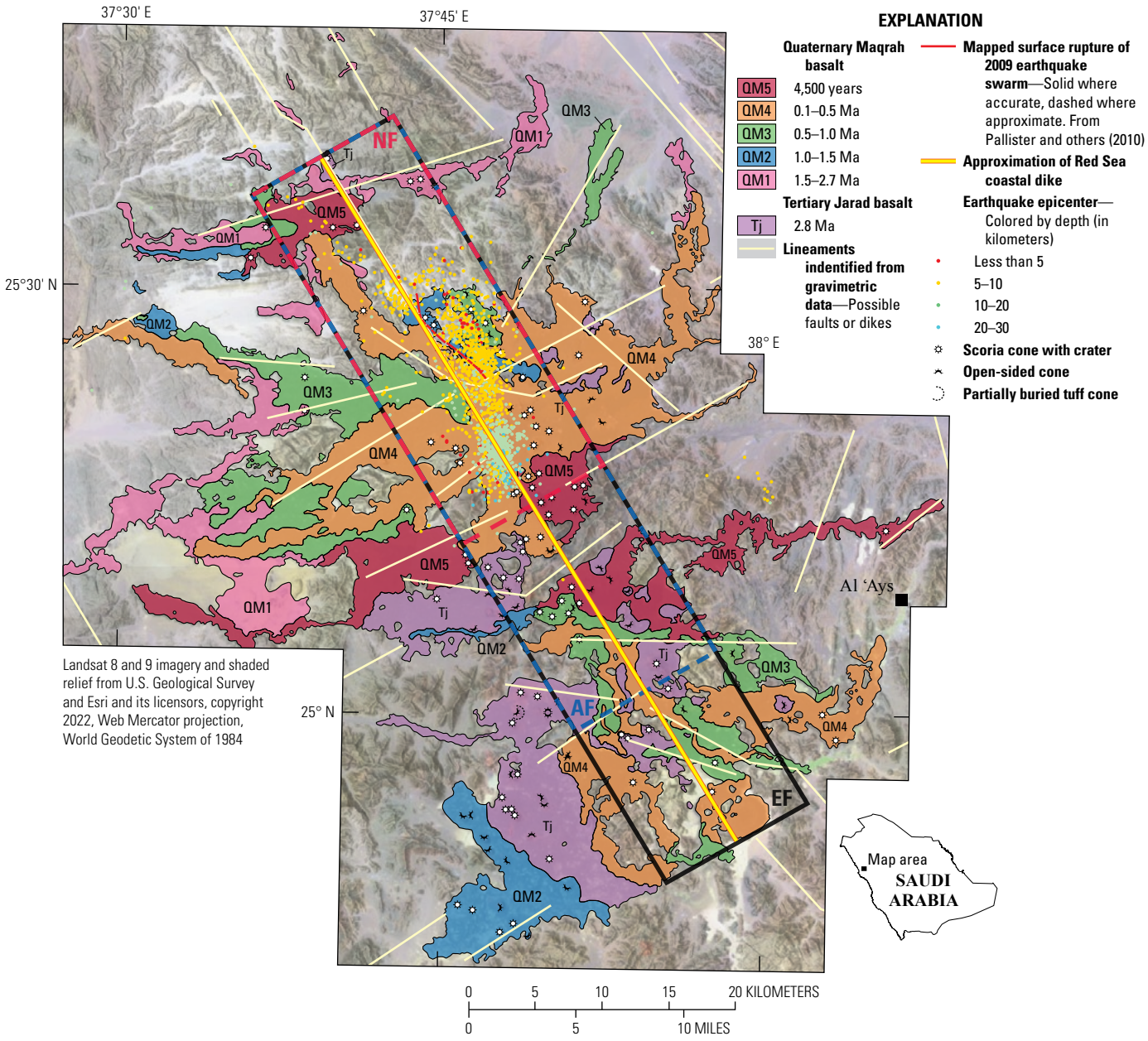

Figure 4. Map of the Harrat Lunayyir area in western Saudi Arabia showing the location of swarm zones corresponding to three regions of swarm localization (see text): the north section of the coastal dike (NF, outlined in red), the active section of the coastal dike (AF, outlined in blue), and the entire coastal dike (EF, outlined in black). Note that the active section also includes the north section, and the entire section includes both the active and the north sections. The line along the long axis of the three swarm zones approximates the location of the coastal dike. Geology and seismicity from Zahran and El-Hady (2017); geologic map modified from Al-Amri and others (2012) by Zahran (2017). Lava field ages (in mega-annum [Ma]) are shown by different colors.

of the particular swarm volume inside the considered swarm zone (fig. 4) and the random azimuth of the swarm volume are assigned. Figure 5 shows, as an example, the epicenters of events in three scenario swarms located inside the entire fault (EF) swarm zone. Note that because of randomly chosen characteristics of the scenario swarm and earthquakes, some relatively large magnitude earthquake sources may be similar in dimension to the scenario swarm zones.

Northern Harrat Rahat

Several zones in which scenario earthquake swarms may occur were selected in the northern Harrat Rahat area (fig. 6). Two zones (zones 1 and 2) are located along the so-called "eastern vent axis" (Stelten and others, 2020), a narrow ridge that has the greatest constructional volcanic relief and numerous volcanic cones and vents of different

Table 1. Parameters used for stochastic simulation of the scenario earthquake swarms for the Harrat Lunayyir area, western Saudi Arabia.

[km, kilometer; °, degree; -, not applicable]

Parameter, unit	Range of variation			Distribution law and standard deviation (σ)
	Minimum	Mean	Maximum	
Length (y), km	12	14	16	Truncated normal, σ = 1.0 km
Width (x), km	5	7	9	Truncated normal, σ = 1.0 km
Size along depth (z), km	8	10	12	Truncated normal, σ = 1.0 km
Upper depth, km	2	-	5	Uniform between minimum and maximum depths
Azimuth of the swarm y-axis	-	Strike of dike	-	Normal, σ = 5°
Recurrence rate, b-value	-	0.9	-	Normal, σ = 0.05

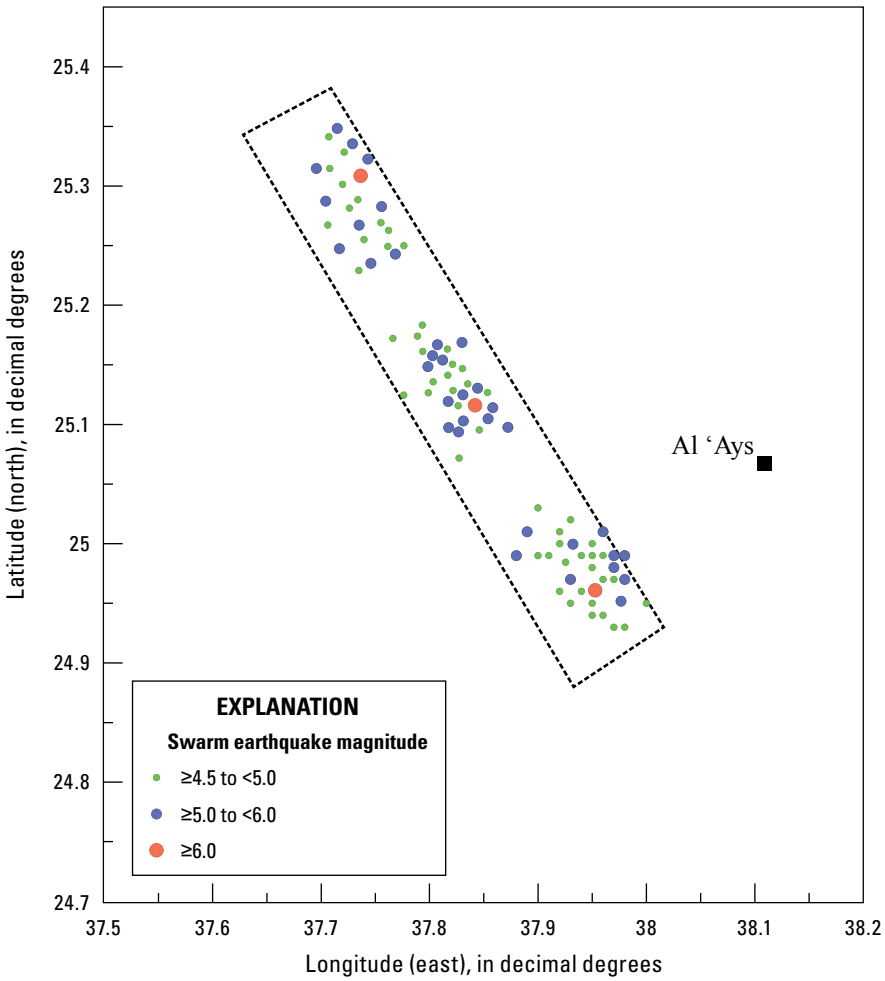

Figure 5. Map plot of three examples of stochastic earthquake swarms showing location of earthquake epicenters generated during three scenarios for the Harrat Lunayyir area in western Saudi Arabia. Dashed line denotes the swarm seismic source zone, using the "entire fault" (EF) model (see also fig. 4).

ages that stretches along major north-northwest trending lineaments. Zone 2 contains several intersections between the major north-northwest trending fault and the east-northeast trending lineaments. A smalller zone (zone 3) with intersections between the north-northwest trending fault and the east-northeast trending lineaments is outlined near the southwest border of zone 2. Finally, a separate zone (zone 4) is delineated in the northwestern part of the area along the west-northwest trending lineaments and around their intersection with an east-northeast trending lineament. Zone 4 contains epicenters of a few small (<*M*3) earthquakes and a north-northwest aligned chain of four small, non-eroded cinder cones and short lava flows that are separate from the contiguous Harrat Rahat. These young-appearing cones and flows were provisionally interpreted to have erupted in 641 C.E. (Camp and Roobol, 1989), but direct age measurements indicate they erupted about 13,400 years ago (Downs and others, 2018; Stelten and others, 2020).

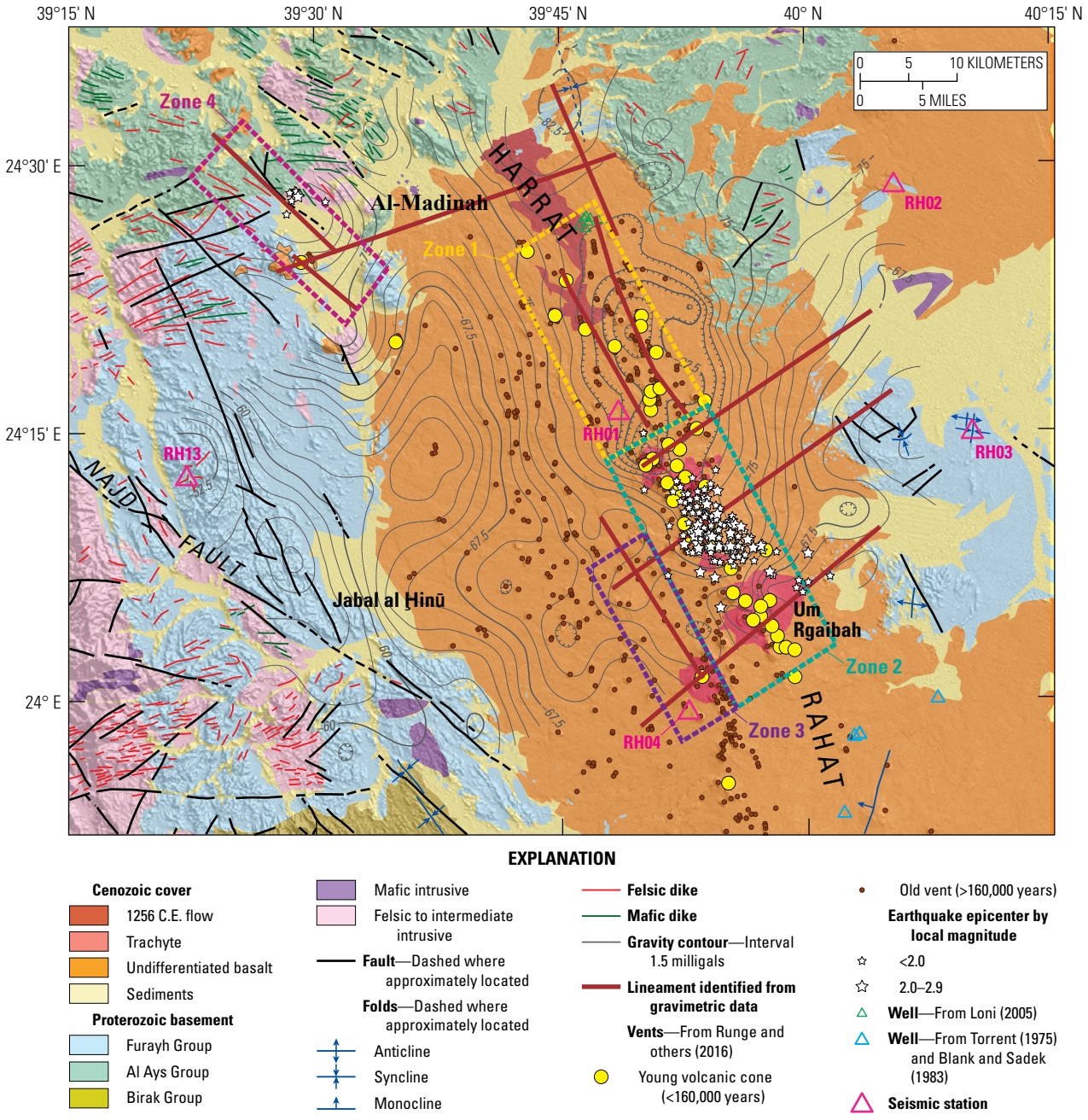

Figure 6. Simplified geologic map of northern Harrat Rahat in western Saudi Arabia, showing the locations of swarm zones 1–4. Modified from Langenheim and others (2019).

Maximum magnitudes for every scenario swarm are considered as random variables with a uniform distribution varying within the range $M_{max}-\Delta M$, where ΔM is uncertainty and equals 0.25. Several alternative models of swarm source zones may be constructed for the area. In this work we show calculations based on the most complex model of earthquake swarm source zones that is characterized by the largest number of source zones (four swarm zones) and by relatively large maximum magnitudes. The maximum magnitudes are assigned for the northern Harrat Rahat swarm zones as follows: zone 1—M_w 6.0; zone 2—M_w 6.4; zone 3—M_w 6.0; and zone 4—M_w 6.0; a ΔM value of 0.25 is assumed for all zones. The other parameters used for stochastic generation of the scenario swarms are taken as those assumed for the case of the Harrat Lunayyir area (table 1).

Procedure, Results, and Discussion

Harrat Lunayyir Area

The calculation involves the generation of 1,500 scenario swarms distributed within each model of the Harrat Lunayyir swarm zones (fig. 4) and the number of swarms is directly proportional to the area of a given zone. Ground-motion parameters are calculated from all earthquakes for a region with dimensions 200 km × 200 km around the swarm source zones on a grid 10 km × 10 km and specifically for location of the town of Al ʻAys. The logic tree scheme is the same as the one applied for calculation of the PSHA for the Harrat Lunayyir volcanic area (Zahran and El-Hady, 2017). First, the ground-motion prediction model developed for the volcanic region of Hawai‘i by Atkinson (2010) is considered with the largest weight (0.4). Second, the model of Atkinson and Boore (2006) (weight 0.2) that was developed for stable continental regions is used in conjunction with the equations for active shallow crustal sources, namely: the models of Zhao and others (2006) (weight 0.1), Boore and Atkinson (2008) (weight 0.1), Campbell and Bozorgnia (2008) (weight 0.1), and Akkar and others (2014) (weight 0.1).

The PGA values are estimated using equations 1 and 2 for three typical site conditions using the site classification accepted in the Saudi Building Code (SBC 301-CR-18, chapter 20; Saudi Building Code National Committee, 2018). The site conditions are the following: (1) class B or rock site—average shear wave velocity of the top 30 m of the soil column (V_{S30}) ranges from 760 to 1,520 m/s (a value of 800 m/s is used); (2) class C or very dense soil—V_{S30} ranges from 360 to 760 m/s (a value of 500 m/s is used); and (3) class D or stiff soil—V_{S30} ranges from 180 to 360 m/s (a value of 300 m/s is used).

The accumulated set of ground-motion values for every location is used for construction and analysis of the probability distribution function and cumulative distribution function for ground-motion levels given distribution of magnitudes and hypocenters of possible swarm earthquakes. The distribution functions obtained considering all ground-motion estimations are influenced by numerous data from distant and small events. Therefore, we use the technique suggested by Sokolov (2017) that implies consideration of the distribution of the parameter values A above a certain threshold level A_0. The technique is briefly described below, and further detailed by Sokolov (2017).

First, we denote the cumulative distribution function, that is, the probability of non-exceedance, for random values a above the certain threshold level A_0 as $F_{A_0}(a) = P(A \le a|A_0)$; the function varies from 0 for $a = A_0$ to about 1 at sufficiently large values of a. Correspondingly, the complementary cumulative distribution function, that is, probability of exceedance, is denoted as $FC_{A_0}(a) = P(A > a|A_0) = 1 - F_{A_0}(a)$; the function varies from 1 to about 0.

Second, we assume that the macroseismic intensity may be used as a simple characteristic of earthquake damage. Sokolov (2017) suggested considering relations between macroseismic intensity and ground-motion parameters (so-called intensity to ground-motion conversion equations) for the selection of threshold level A_0 and the construction of the cumulative distribution functions. In terms of the Modified Mercalli Intensity (MMI) scale, macroseismic intensity MMI V characterizes the lowest level of ground motion (moderate shaking) for which damage to ordinary buildings may occur. Thus, the threshold level may be assumed to be the level of ground motion that corresponds to intensity MMI V, that is $A_0 = A_{MMI\,V}$. From this point of view, the higher the level of ground motion exceeding the threshold level, the larger degree of possible damage. Note that Atkinson (2015) suggested considering MMI VI (strong shaking) as the lower bound threshold for potential damage. Thus, selection of the proper threshold (MMI V or VI) may depend on the user's opinion and goal of their study, such as estimation of the hazard for ordinary buildings or critical structures.

Third, considering the relation between the level of ground motion and possible damage, Sokolov (2017) suggests a special term for the value of ground motion a above the threshold level that may be exceeded with a particular probability $P(A > a|A_{MMI\,V})$. If the result of the hazard assessment is used for design purposes, the value a represents the "N-percent-damage" ground-motion parameter. Here, N denotes the probability of exceedance $P(A > a|A_{MMI\,V})$ expressed as a percentage, for example 10 percent or 5 percent. It means that if numerous swarm earthquakes occur around the site of interest, the intensity of ground shaking during 10 percent (or 5 percent) of the events will be larger than the considered ground motion level a. As mentioned by Sokolov (2017), the term "N-percent-damage" does not describe in a quantitative manner the expected degree of damage for particular structures that experience ground motion level A. The degree of damage has to be estimated using construction-specific fragility functions for a given ground-motion intensity. Alternatively, the term "safety" may be used instead of the term "damage." In this case, the ground-motion level a selected for a specified probability of non-exceedance

$P(A \leq a|A_{MMI\ V})$ may be called the "*N*-percent-safety" ground-motion parameter, for example 95-percent-safety.

Seismic intensity on a macroseismic scale is expressed in Roman numerals, whereas the conversion equations consider decimal numbers—the so-called instrumental intensity values. Therefore, any given value of seismic intensity (Roman numeral) corresponds to a range of instrumental intensity values. For example, seismic intensity VI corresponds to instrumental intensity values greater than 5.5–6.5. Let us also consider the lower value of instrumental intensity that can characterize the MMI value; for example, instrumental intensity = 4.6 for MMI V. There are several MMI-PGA relations, among which we mention the following. Worden and others (2012) obtained $PGA_{MMI\ V}$ = 60 cm/s^2 for California earthquakes; this relatively high value reflects advanced seismic design standards in the region. Bilal and Askan (2014) analyzed Turkish data based on the building stock mostly not complying with the current seismic regulations and their MMI-PGA relation resulted in a $PGA_{MMI\ V}$ of about 15 cm/s^2. Mohindra and others (2012) provided the MMI-PGA relation for the building stock in Yemen, and the relation results in a $PGA_{MMI\ V}$ of about 20 cm/s^2. The $PGA_{MMI\ V}$ was estimated by Chernov (1989) as 25 cm/s^2 based on data from across the globe. Chernov's (1989) PGA-MMI relation is outdated; however, it was obtained independently of a particular region and quality of construction and, therefore, it may be considered, to the first approximation, as an average relation. Note that the value of 25 cm/s^2 is approximately equal to the mean value of other estimations shown above, namely: 60 cm/s^2, 15 cm/s^2, and 20 cm/s^2.

In this study, we use the threshold value $A_{MMI\ V}$ = 25 cm/s^2 and the corresponding probability density function and cumulative probability function constructed for the town of Al 'Ays are shown in figure 7*A*. Figure 7*B* shows the distribution of PGA values (site class B, rock) along the studied area. The PGA values are estimated for 90 percent probability that the ground-motion value above the threshold value of 25 cm/s^2 will not be exceeded; for example,

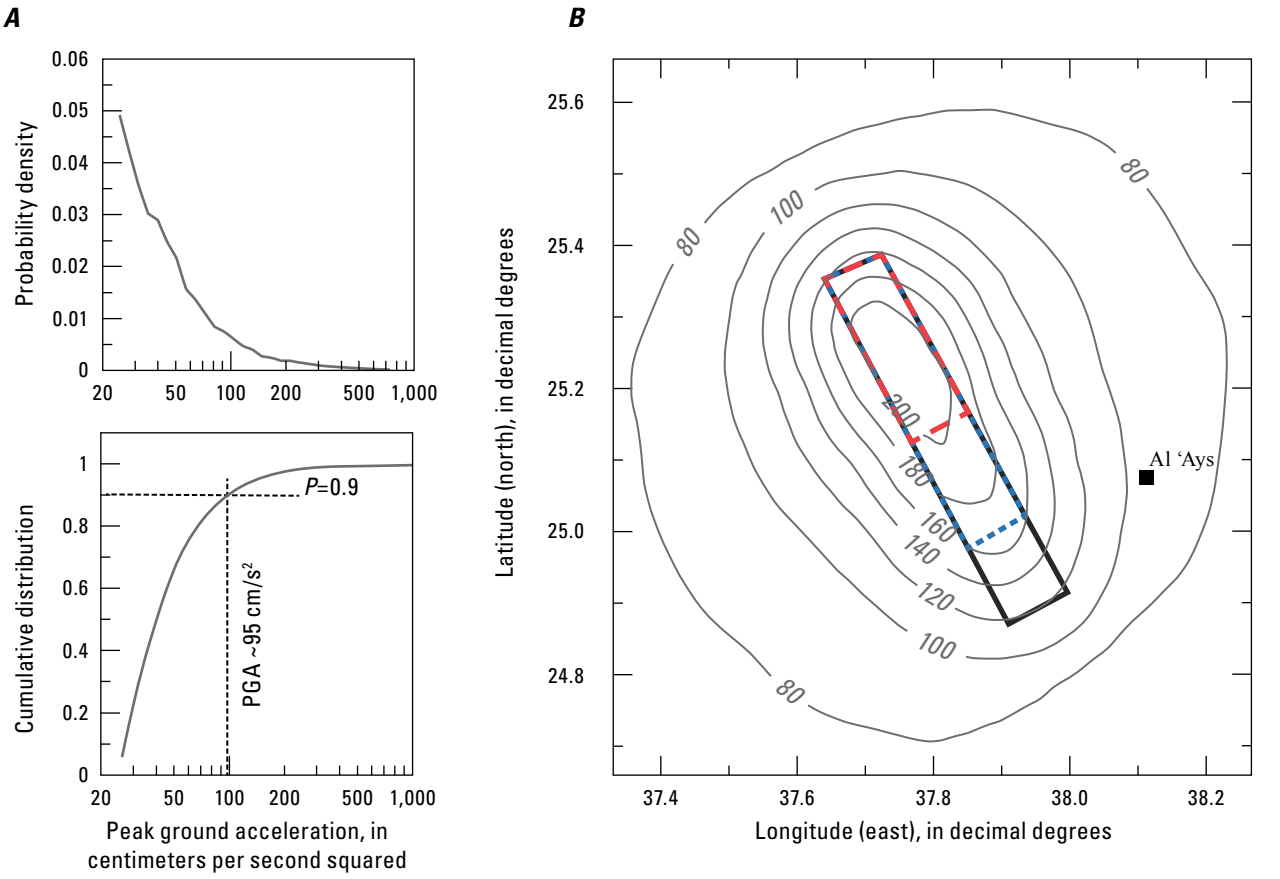

Figure 7. Plots showing the results of a scenario-based earthquake swarm hazard assessment for the Harrat Lunayyir area in western Saudi Arabia. *A*, Probability density functions and cumulative probability functions for peak ground acceleration (PGA) values above the threshold level (25 centimeters per second squared [cm/s^2]) for site class B near the town of Al 'Ays. *B*, Distribution of PGA (in cm/s^2) for site class B calculated for 90 percent probability that the ground-motion values above the threshold level will not be exceeded; that is, $P(A \leq a|25\ cm/s^2) = 0.9$, where *P* is probability, *A* is the ground-motion value, and *a* is the possible ground-motion value above the threshold level. Dashed lines show location of the swarm zones that correspond to three variants of swarm localization: red outlines the north section of the fault, blue the active section of the fault, and black the entire fault (fig. 4).

$P(A \leq a|25\ \text{cm/ s}^2) = 0.9$. As expected, the maximum estimated PGA values are concentrated in the northern part of the entire swarm zone.

The representation of seismic hazard from earthquake swarms in the form of probability functions allows flexible selection of ground-motion levels considering appropriate probability of exceedance (or non-exceedance). The question of what probability is best for design or risk-mitigation purposes requires special studies that may include consideration of issues related to seismic risk assessment. In this study, we present a comparison of our estimations with the results of a PSHA that was performed recently for the study area (Zahran and El-Hady, 2017). The comparison may be considered as an instructive first attempt and an example of how to determine the appropriate level of probability.

The results of the hazard assessments for different site conditions for the town of Al ʻAys are listed in table 2. As shown in the table, the estimations based on consideration of swarm earthquakes and obtained for 80 percent and 95 percent probability that the ground-motion value above the threshold value of 25 cm/s^2 will not be exceeded (for example, 80- and 95-percent-safety levels), approximately correspond to the PSHA estimations (Zahran and El-Hady, 2017) for return periods of 475 years and 2,475 years, respectively. Note that PGA values of more than 140 cm/s^2 are assigned for the Harrat Lunayyir area in the recent edition of the Saudi Building Code that assumes a return period of 2,475 years (see fig. 22-3 of SBC 301-CR-18; Saudi Building Code National Committee, 2018).

Harrat Rahat Area

Results of the similar scenario-based earthquake swarm seismic hazard assessment for the northern Harrat Rahat area (PGA for $P(A \leq a|25\ \text{cm/s}^2) = 0.9$, site class B) are shown in figure 8. Maximum estimated PGA values are concentrated near the centers of the swarm zones. By comparison, the recent edition of the Saudi Building Code assigns PGA values of about 80 cm/s^2 for the territory of Harrat Rahat (see fig. 22-3 of SBC 301-CR-18).

When comparing the results of seismic hazard estimations obtained by a conventional PSHA (for example, seismic hazard maps used for developing building codes) with our approach that uses stochastic estimates generated for an earthquake swarm, we consider the following caveats. First, the uncertainties in earthquake recurrence parameters, especially in the overall rate of earthquakes (*a*-value), may greatly affect the results of the PSHA. Second, the stochastic modeling of earthquake swarms considers only the relative ratio of small and large magnitudes (*b*-value) and a fixed number of the largest magnitude events. The backward calculation of the number of earthquakes that have smaller magnitudes using varying *b*-values would result in a different estimate of the number of the earthquakes in each scenario generated. However, the number of relatively large events (earthquakes with magnitudes close to the maximum magnitude) would be approximately the same. Consequently, the results of any seismic hazard assessment based on a sufficiently large number of earthquake swarm scenarios, besides the accepted probability of non-exceedance, depend mostly on the assumed maximum magnitudes and size of the possible swarm zones. If a number of alternative swarm zone models are considered, the weighting scheme may contribute uncertainty to the results.

In addition, the swarms may contain several intermediate-size earthquakes that would be removed during declustering, which is a necessary procedure in a PSHA. Thus, influence of such earthquakes would not be considered in a PSHA. In contrast, in the stochastic modeling of earthquake swarms, intermediate-size earthquakes do contribute to ground-motion probability distribution functions. Thus, the swarm generation analysis may supplement the results of a standard PSHA.

We note that another possibility for assessing seismic hazard from an earthquake swarm is the consideration of only the maximum earthquake magnitude in each swarm scenario. Such an approach is broadly consistent with the technique suggested by Sokolov (2017) for evaluation of seismic hazard from maximum magnitude earthquakes. In this case, estimation of ground motion may be considered the "maximum credible" estimation showing the upper bound of the anticipated ground-motion intensity.

Table 2. Results of the scenario-based earthquake swarm hazard assessment for the town of Al ʻAys, Saudi Arabia, near Harrat Lunayyir showing peak ground acceleration (PGA) estimations for different probabilities of non-exceedance $P(A \leq a|A_{\text{MMI V}})$, where $A_{\text{MMI V}} = 25$ cm/s^2.

[Values in centimeters per second squared (cm/s^2). *P*, probability; *a*, possible ground-motion value above the threshold level; *A*, ground-motion value; $A_{\text{MMI V}}$, threshold for moderate shaking at Modified Mercalli Intensity level V; %, percent; PSHA, probabilistic seismic hazard assessment]

Site condition (site class)	Peak ground acceleration (PGA)				
	***P* = 80.0%**	***P* = 90.0%**	***P* = 95.0%**	***P* = 99.0%**	***P* = 99.5%**
Rock (B)	70 (60)[a]	95	145 (150)[b]	290	380
Very dense soil (C)	75 (70)[a]	105	160 (170)[b]	320	395
Stiff soil (D)	80 (80)[a]	120	175 (200)[b]	360	460

[a]Values in parentheses show PSHA estimations obtained for return periods of 475 years (Zahran and El-Hady, 2017).

[b]Values in parentheses show PSHA estimations obtained for return periods of 2,475 years (Zahran and El-Hady, 2017).

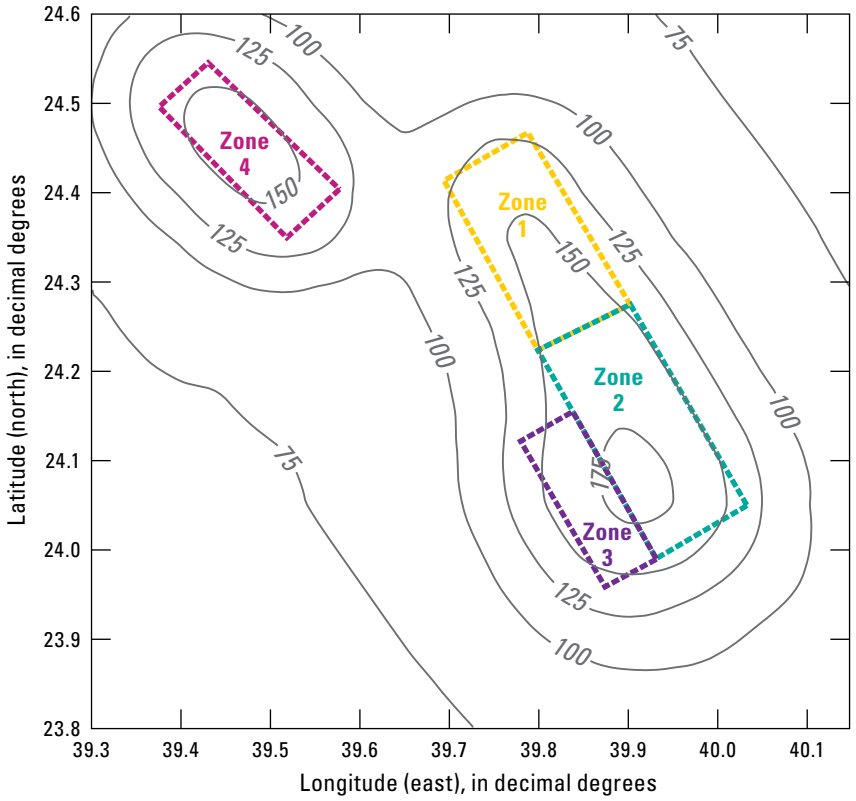

Figure 8. Map plot of the northern Harrat Rahat area, western Saudi Arabia, showing the distribution of peak ground acceleration (in centimeters per second squared [cm/s^2]) for site class B, calculated for 90 percent probability that the threshold value of 25 cm/s^2 will not be exceeded; that is, $P(A \leq a|25\ \text{cm/s}^2) = 0.9$, where P is probability, A is the ground-motion value, and a is the possible ground-motion value above the threshold level. Dashed lines show location of swarm zones 1–4 (see also fig. 6).

Conclusions

Earthquake swarms caused by natural processes or triggered by human activity may represent a considerable source of risk for nearby settlements. Standard probabilistic seismic hazard analysis considers independent, time-independent earthquakes, therefore the influence of numerous, temporally chaotic seismic events in a swarm are not taken into account. The alternative deterministic approach is based on a few specific earthquake scenarios assuming a maximum magnitude and shortest distance to the site of interest. However, this approach may provide an unreasonably high estimated level of seismic hazard.

In this work, we describe a scenario-based approach for the estimation of seismic hazard from seismic swarms. We use as examples two active lava fields: Harrat Lunayyir and northern Harrat Rahat, both located in western Saudi Arabia. The areas have experienced repeated volcanic activity and episodic seismic swarm activity believed to be caused by the intrusion of magma into the crust.

The scenario approach used here assumes the stochastic generation of a large number of seismic swarms with randomly varying physical characteristics (location of the swarm, maximum magnitude, the ratio between the maximum magnitude earthquake and earthquakes that have smaller magnitudes). Ground-motion parameters at a site of interest are calculated from all events in all swarms and the corresponding probability distribution function of ground-motion parameters are analyzed. The level of ground motion may be selected considering appropriate value of probability of exceedance that, in turn, depends on the engineering objective of the study.

Bearing in mind the assumptions of the method, the swarm generation analysis suggested here may provide a valuable supplement to the results of an ordinary probabilistic seismic hazard assessment (PSHA). For example, the earthquake swarm activity in Harrat Lunayyir and northern Harrat Rahat is associated with geological faults and (or) dikes. Therefore, it is advisable to estimate the effects of large (maximum credible magnitude) earthquakes that may occur along these geological structures (Zahran and others, 2019). We have described our methodology for seismic hazard assessment of earthquake swarms for a specific volcanic region of northwestern Saudi Arabia. However, the technique may be applied to other areas throughout the world where earthquake swarms, with either a tectonic or induced origin, may occur.

Acknowledgments

We are grateful to Walter D. Mooney for detailed and constructive comments that greatly improved the initial manuscript. We also thank Arthur Frankel and Ryota Kiuchi for their reviews of the manuscript and their comments. The work has been performed in the National Center for Earthquakes and Volcanoes, Saudi Geological Survey, Jiddah, Kingdom of Saudi Arabia, under a cooperative agreement between the U.S. Geological Survey and Saudi Geological Survey.

References Cited

Abdelfattah, A.K., de Lorenzo, S., Almadani, S., Fnais, M., Alfaifi, H., and Al-Arifi, N., 2019, Another look at the 2009 seismic activity, Harrat Lunayyir, Saudi Arabia: Journal of Seismology, v. 23, p. 801–818, https://doi.org/10.1007/s10950-019-09835-0.

Abdelfattah, A.K., Mogren, S., and Mukhopadhyay, M., 2017, Mapping b-value for 2009 Harrat Lunayyir earthquake swarm, western Saudi Arabia and Coulomb stress for its mainshock: Journal of Volcanology and Geothermal Research, v. 330, p. 14–23, https://doi.org/10.1016/j.jvolgeores.2016.12.001.

Abdelwahed, M.F., El-Masry, N., Moufti, M.R., Kenedi, C.L., Zhao, D., Zahran, H., and Shawali, J., 2016, Imaging of magma intrusions beneath Harrat Al-Madinah in Saudi Arabia: Journal of Asian Earth Sciences, v. 120, p. 17–28, https://doi.org/10.1016/j.jseaes.2016.01.023.

Akkar, S., Sandikkaya, M.A., and Bommer, J.J., 2014, Empirical ground-motion models for point- and extended-source crustal earthquake scenarios in Europe and the Middle East: Bulletin of Earthquake Engineering, v. 12, p. 359–387, https://doi.org/10.1007/s10518-013-9461-4.

Al-Amri, A.M., Fnais, M.S., Abdel-Rahman, K., Mogren, S., and Al-Dabbagh, M., 2012, Geochronological dating and stratigraphic sequences of Harrat Lunayyir, NW Saudi Arabia: International Journal of Physical Sciences, v. 7, no. 20, p. 2791–2805, accessed December 18, 2022, at https://academicjournals.org/journal/IJPS/article-full-text-pdf/D950EAB19041.

Al-Arifi, N.S., Fat-Helbary, R.E., Khalil, A.R., and Lashin, A.A., 2013, A new evaluation of seismic hazard for the northwestern part of Saudi Arabia: Natural Hazards, v. 69, p. 1435–1457, https://doi.org/10.1007/s11069-013-0756-1.

Albaric, J., Perrot, J., Déverchère, J., Deschamps, A., Le Gall, B., Ferdinand, R.W., Petit, C., Tiberi, C., Sue, C., and Songo, M., 2010, Contrasted seismogenic and rheological behaviours from shallow and deep earthquake sequences in the North Tanzanian Divergence, East Africa: Journal of African Earth Sciences, v. 58, p. 799–811, https://doi.org/10.1016/j.jafrearsci.2009.09.005.

Ambraseys, N.N., 1988, The seismicity of Saudi Arabia and adjacent areas: Imperial College, London, Engineering Seismology and Earthquake Engineering publication no. 88/11, 294 p.

Ambraseys, N.N., and Melville, C.P., and Adams, R.D., 1994, The seismicity of Egypt, Arabia, and the Red Sea: Cambridge University Press, 182 p.

Atkinson, G.M., 2010, Ground-motion prediction equations for Hawaii from a referenced empirical approach: Bulletin of the Seismological Society of America, v. 100, no. 2, p. 751–761, https://doi.org/10.1785/0120090098.

Atkinson, G.M., 2015, Ground-motion prediction equation for small-to-moderate events at short hypocentral distances, with application to induced-seismicity hazard: Bulletin of the Seismological Society of America, v. 105, no. 2A, p. 981–992, https://doi.org/10.1785/0120140142.

Atkinson, G.M., and Boore, D.M., 2006, Earthquake ground-motion prediction equations for Eastern North America: Bulletin of Seismological Society of America, v. 96, no. 6, p. 2181–2205, https://doi.org/10.1785/0120050245.

Baer, G., and Hamiel, Y., 2010, Form and growth of an embryonic continental rift—InSAR observations and modelling of the 2009 western Arabia rifting episode: Geophysical Journal International, v. 182, p. 155–167, https://doi.org/10.1111/j.1365-246X.2010.04627.x.

Bilal, M., and Askan, A., 2014, Relationships between felt intensity and recorded ground-motion parameters for Turkey: Bulletin of the Seismological Society of America, v. 104, p. 484–496, https://doi.org/10.1785/0120130093.

Boore, D.M., and Atkinson, G.M., 2008, Ground-motion prediction equations for the average horizontal component of PGA, PGV, and 5%-damped PSA at spectral periods between 0.01 s and 10.0 s: Earthquake Spectra, v. 24, p. 99–138.

Boyd, O.S., 2012, Including foreshocks and aftershocks in time-independent probabilistic seismic-hazard analyses: Bulletin of the Seismological Society of America, v. 102, no. 3, p. 909–917, https://doi.org/10.1785/0120110008.

Brown, G.F., Schmidt, D.L., and Huffman, A.C., Jr., 1989, Geology of the Arabian Peninsula, shield area of western Saudi Arabia: U.S. Geological Survey Professional Paper 560–A, 188 p.

Camp, V.E., 1986, Geologic map of the Umm al Birak quadrangle, sheet 23D, Kingdom of Saudi Arabia (with text): Saudi Arabian Directorate General of Mineral Resources Geologic Map GM-87C, scale 1:250,000, 40 p.

Camp, V.E., Hooper, P.R., Roobol, M.J., and White, D.L., 1987, The Madinah eruption, Saudi Arabia—Magma mixing and simultaneous extrusion of three basaltic chemical types: Bulletin of Volcanology, v. 49, no. 2, p. 489–508, https://doi.org/10.1007/BF01245475.

Camp, V.E., and Roobol, M.J., 1989, The Arabian continental alkali basalt province; Part I—Evolution of Harrat Rahat, Kingdom of Saudi Arabia: Geological Society of America Bulletin, v. 101, p. 71–95, https://doi.org/10.1130/0016-7606(1989)101<0071:TACABP>2.3.CO;2.

Camp, V.E., and Roobol, M.J., 1992, Upwelling asthenosphere beneath western Arabia and its regional implications: Journal of Geophysical Research—Solid Earth, v. 97, no. B11, p. 15255–15271, https://doi.org/10.1029/92JB00943.

Campbell, K.W., and Bozorgnia, Y., 2008, NGA ground motion model for the geometric mean horizontal component of PGA, PGV, PGD and 5% damped linear elastic response spectra for periods ranging from 0.01 s to 10 s: Earthquake Spectra, v. 24, p. 139–171, https://doi.org/10.1193/1.2857546.

Chan, C.-H., Wu, Y.-M., Cheng, C.-T., Lin, P.-S., and Wu, Y.-C., 2013, Time-dependent probabilistic seismic hazard assessment and its application to Hualien City, Taiwan: Natural Hazards and Earth System Sciences, v. 13, p. 1143–1158, https://doi.org/10.5194/nhess-13-1143-2013.

Chen, J., and Wolf, L.W., 2018, A notable earthquake swarm in Alabama—Natural or anthropogenic?: Seismological Research Letters, v. 89, no. 4, p. 1583–1594, https://doi.org/10.1785/0220170284.

Chernov, Y.K., 1989, Strong ground motion and quantitative assessment of seismic hazard: Fan Publishing House, Tashkent [in Russian].

Downs, D.T., Stelten, M.E., Champion, D.E., Dietterich, H.R., Nawab, Z., Zahran, H., Hassan, K., and Shawali, J., 2018, Volcanic history of the northernmost part of the Harrat Rahat volcanic field, Saudi Arabia: Geosphere, v. 14, no. 3, p. 1253–1282, https://doi.org/10.1130/GES01625.1.

Duncan, R.A., and Al-Amri, A.M., 2013, Timing and composition of volcanic activity at Harrat Lunayyir, western Saudi Arabia: Journal of Volcanology and Geothermal Research, v. 260, p. 103–116, https://doi.org/10.1016/j.jvolgeores.2013.05.006.

El-Masry, N.N., Moufti, M.R.H., Nemeth, K., Murcia, H., Qaddah, A.A., and Abdelwahed, M.F., 2013, Historical accounts of the AD 1256 eruption near Al-Madinah: Proceedings of the VORiSA scientific meeting, King Abdulaziz University, Jiddah, November 17–18, p. 9–13, https://doi.org/10.13140/RG.2.1.4493.9602.

Gutenberg, B., and Richter, C.F., 1956, Magnitude and energy of earthquakes: Annali di Geofisica, v. 9, p. 1–15, https://doi.org/10.4401/ag-5590.

Kenedi, C.L., Runge, M.G., Mokhtar, T.A., Abdelwahed, M.F., and Lindsay, J.M., 2013, The 1256 & 1999 Harrat Rahat and 2009 Lunayyir earthquake swarms—Implication for future volcano-seismic activity in Al-Madinah: Proceedings of the VORiSA scientific meeting, King Abdulaziz University, Jiddah, November 17–18, p. 102–106.

Kijko, A., and Graham, G., 1998, Parametric-historic procedure for probabilistic seismic hazard analysis Part I—Estimation of maximum regional magnitude mmax: Pure and Applied Geophysics, v. 152, p. 413–442, https://doi.org/10.1007/s000240050161.

Langenheim, V.E., Ritzinger, B.T., Zahran, H., Shareef, A., and Al-dahri, M., 2019, Crustal structure of the northern Harrat Rahat volcanic field (Saudi Arabia) from gravity and aeromagnetic data: Tectonophysics, v. 750, p. 9–21, https://doi.org/10.1016/j.tecto.2018.11.005.

Livaoğlu, R., Timurağaoğlu, M.Ö., Serhatoğlu, C., and Döven, M.S., 2017, Damages during February, 6–24 2017 Çanakkale earthquake swarm: Natural Hazards and Earth System Sciences Discussion, https://doi.org/10.5194/nhess-2017-245.

Marzocchi, W., and Taroni, M., 2014, Some thoughts on declustering in probabilistic seismic-hazard analysis: Bulletin of the Seismological Society of America, v. 104, no. 4, p. 1838–1845, https://doi.org/10.1785/0120130300.

Mohindra, R., Nair, A.K.S., Gupta, S., Sur, U., and Sokolov, V., 2012, Probabilistic seismic hazard analysis for Yemen: International Journal of Geophysics, article no. 304235, https://doi.org/10.1155/2012/304235.

Mokhtar, T.A., Shawali, J.A., Abdelwahed, M.F., Runge, G.M., and Kenedi, C.L., 2013, The 1999 micro-earthquake swarms of northern Harrat Rahat: Proceedings of the VORiSA scientific meeting, King Abdulaziz University, Jiddah, November 17–18, p. 69–72.

Moufti, M.R., Németh, K., Murcia, H., and Lindsay, J.M., 2013, The 1256 AD Al Madinah historic eruption geosite as the youngest volcanic chain in the Kingdom of Saudi Arabia: International Journal of Earth Sciences, v. 102, no. 4, p. 1069–1070, https://doi.org/10.1007/s00531-013-0878-4.

Mukhopadhyay, B., Mogren, S., Mukhopadhyay, M., and Dasgupta, S., 2013, Incipient status of dyke intrusion in top crust—Evidences from the Al-Ays 2009 earthquake swarm, Harrat Lunayyir, SW Saudi Arabia: Geomatics, Natural Hazards and Risk, v. 4, p. 30–48, https://doi.org/10.1080/19475705.2012.663794.

Pallister, J.S., McCausland, W.A., Jónsson, S., Lu, Z., Zahran, H.M., Hadidy, S.E., Aburukbah, A., Stewart, I.C.F., Lundgren, P.R., White, R.A., and Moufti, M.R.H., 2010, Broad accommodation of rift-related extension recorded by dike intrusion in Saudi Arabia: Nature Geoscience, v. 3, p. 705–712, https://doi.org/10.1038/ngeo966.

Pellaton, C., 1981, Geologic map of the Al Madinah quadrangle, Sheet 24D, Kingdom of Saudi Arabia (with text): Saudi Arabian Directorate General of Mineral Resources Geologic Map GM-52C, scale 1:250,000, 19 p.

Roobol, M.J., and Al-Rehaili, M., 1997, Geohazards along the Makkah–Madinah–Nafud (MMN) volcanic line: Saudi Arabian Deputy Ministry for Mineral Resources Technical Report DMMR-TR-97-1, p. 125–140.

Roobol, M.J., and Camp, V.E., 1991, Geology of the Cenozoic lava field of Harrats Khaybar, Ithnayn, and Kura: Saudi Arabian Directorate General of Mineral Resources Geoscience Map GM-131, scale 1:250,000, pamphlet 76 p.

Roobol, M.J., and Kadi, K.A., 2008, Cenozoic faulting in the Rabigh area, central west Saudi Arabia (including the sites of King Abdullah Economic City and King Abdullah University for Science and Technology): Saudi Geological Survey Technical Report SGS–TR–2008–6, scale 1:250,000, pamphlet 12 p.

Roobol, M.J., and Stewart, I.C.F., 2009, Cenozoic faults and recent seismicity in northwest Saudi Arabia and the Gulf of Aqaba region: Saudi Geological Survey Technical Report SGS-TR-2008-7, 35 p., 10 plates.

Saibi, H., Mogren, S., Mukhopadhyay, M., and Ibrahim, E., 2019, Subsurface imaging of the Harrat Lunayyir 2007–2009 earthquake swarm zone, western Saudi Arabia, using potential field methods: Journal of Asian Earth Sciences, v. 169, p. 79–92, https://doi.org/10.1016/j.jseaes.2018.07.024.

Saudi Building Code National Committee, 2018, Saudi Building Code for Loading and Forces, SBC 301-CR-18: Saudi Building Code National Committee: Riyadh, Kingdom of Saudi Arabia, 355 p.

Siebert, L., Simkin, T., and Kimberly, P., 2010, Volcanoes of the world (3rd ed.): Berkeley, University of California Press, 551 p.

Sokolov, V., 2017, Seismic hazard analysis based on maximum credible earthquakes: Bulletin of Earthquake Engineering, v. 15, no. 5, p. 1831–1852, https://doi.org/10.1007/s10518-016-0059-5.

Sokolov, V., and Zahran, H.M., 2018, Seismic hazard analysis for development of risk-targeted ground-motion maps in the western Saudi Arabia: Proceedings of the 16th European Conference on Earthquake Engineering, June18–21, Thessaloniki, Greece.

Sokolov, V., Zahran, H.M., Youssef, S.E-H., El-Hadidy, M., and Alraddadi, W.W., 2017, Probabilistic seismic hazard assessment for Saudi Arabia using spatially smoothed seismicity and analysis of hazard uncertainty: Bulletin of Earthquake Engineering, v. 15, p. 2695–2735, https://doi.org/10.1007/s10518-016-0075-5.

Špičák, A., 2000, Earthquake swarms and accompanying phenomena in intraplate regions—A review: Studia Geophysica et Geodaetica, v. 44, no. 2, p. 89–106.

Stelten, M.E., Downs, D.T., Champion, D.E., Dietterich, H.R., Calvert, A.T., Sisson, T.W., Mahood, G.A., and Zahran, H., 2020, The timing and compositional evolution of volcanism within northern Harrat Rahat, Kingdom of Saudi Arabia: Geological Society of America Bulletin, v. 132, no. 7–8, p. 1381–1403, https://doi.org/10.1130/B35337.1.

Stewart, I.C.F., and Miller, D.T., 2018, Directional tilt derivatives to enhance structural trends in aeromagnetic grids: Journal of Applied Geophysics, v. 159, p. 553–563, https://doi.org/10.1016/j.jappgeo.2018.10.004.

Toro, G.R., and Silva, W.J., 2001, Scenario earthquakes for Saint Louis, MO, and Memphis, TN, and seismic hazard maps for the central United States region—Including the effect of site conditions: Technical report to U.S. Geological Survey under contract 1434-HQ-97-GR-02981, accessed December 18, 2022, at http://www.ce.memphis.edu/7137/PDFs/attenuations/nmsz_risk_report.pdf.

Vakov, A.V., 1996, Relationships between earthquake magnitude, source geometry and slip mechanism: Tectonophysics, v. 261, no. 1–3, p. 97–113, https://doi.org/10.1016/0040-1951(96)82672-2.

van Stiphout, T., Zhuang, J., and Marsan, D., 2012, Seismicity declustering: Community Online Resource for Statistical Seismicity Analysis, 25 p., https://doi.org/10.5078/corssa-52382934.

von Wissman, H., 1963, Arabia and the Indian Ocean, *in* van Padang, M., ed., Catalogue of the active volcanoes of the world including solfatara fields: Rome, International Association of Volcanology, v. 16, p. 3.1-1–3.1-12.

Worden, C.B., Gerstenberger, M.C., Rhoades, D.A., and Wald, D.J., 2012, Probabilistic relationships between ground-motion parameters and modified Mercalli intensity in California: Bulletin of the Seismological Society of America, v. 102, p. 204–221, https://doi.org/10.1785/0120110156.

Yeo, G.L., and Cornell, C.A., 2009, A probabilistic framework for quantification of aftershock ground-motion hazard in California—Methodology and parametric study: Earthquake Engineering and Structural Dynamics, v. 38, no. 1, p. 45–60, https://doi.org/10.1002/eqe.840.

Zahran, H.M., 2017, Seismic hazard assessment in Harrat Lunayyir, western Saudi Arabia: Jiddah, Saudi Arabia, King Abdulaziz University, Ph.D. thesis, 178 p.

Zahran, H.M., and El-Hady, S.M., 2017, Seismic hazard assessment for Harrat Lunayyir—A lava field in western Saudi Arabia: Soil Dynamics and Earthquake Engineering, v. 100, p. 428–444, https://doi.org/10.1016/j.soildyn.2017.06.009.

Zahran, H.M., El-Hady, S.M., and Abuelnaga, H.S., 2017, Aeromagnetic data over Harrat Lunayyir and surrounding areas, western Saudi Arabia: Arabian Journal of Geosciences, v. 10, no. 3, article no. 63, https://doi.org/10.1007/s12517-017-2849-8.

Zahran, H.M., Sokolov, V., and El-Hadidi, S., 2019, Deterministic seismic hazard assessment for the Makkah Region, western Saudi Arabia: Arabian Journal of Geosciences, v. 12, no. 476, https://doi.org/10.1007/s12517-019-4648-x.

Zahran, H.M., Sokolov, V., Roobol, M.J., Stewart, I.C.F., Youssef, S.E-H., and El-Hadidy, M., 2016, On the development of a seismic source zonation model for seismic hazard assessment in western Saudi Arabia: Journal of Seismology, v. 20, no. 3, p. 747–769, https://doi.org/10.1007/s10950-016-9555-y.

Zahran, H.M., Stewart, I.C.F., Johnson, P.R., and Basahel, M.H., 2003, Aeromagnetic-anomaly maps of central and western Saudi Arabia: Saudi Geological Survey Open-File Report SGS–OF–2002–8, 4 sheets, scale 1:2,000,000, 6 p.

Zhao, J.X., Zhang, J., Asano, A., Ohno, Y., Oouchi, T., Takahashi, T., Ogawa, H., Irikura, K., Thio, H.K., Somerville, P.G., Fukushima, Y., and Fukushima, Y., 2006, Attenuation relations of strong ground motion in Japan using site classifications based on predominant period: Bulletin of the Seismological Society of America, v. 96, no. 3, p. 898–913, https://doi.org/10.1785/0120050122.

Zobin, V.M., 2001, Seismic hazard of volcanic activity: Journal of Volcanology and Geothermal Research, v. 112, no. 1–4, p. 1–14, https://doi.org/10.1016/S0377-0273(01)00230-X.

Moffett Field Publishing Service Center, California
Manuscript approved March 22, 2023
Edited by Lisa Rukstales and Monica Erdman
Layout and design by Kimber Petersen
Illustration support by Katie Sullivan

ISSN 1044-9612 (print)
ISSN 2330-7102 (online)
https://doi.org/10.3133/pp1862P